Colloid and Polymer Science (2024) 302:1957–1966
https://doi.org/10.1007/s00396-024-05320-4

RESEARCH

Multicompartment microparticles of SBM triblock terpolymers: Morphological transitions through homopolymer blending

Manuel Trömer[1] · Arash Nikoubashman[2,3] · André H. Gröschel[1,4]

Received: 17 June 2024 / Revised: 26 August 2024 / Accepted: 30 August 2024 / Published online: 17 September 2024

Abstract

Block copolymers (BCPs) have recently been explored in spherical confinement to form internally structured microparticles. While the behavior of AB diblock copolymers in confinement is comparably well studied, knowledge on confined ABC triblock terpolymers is still rather sparse. The latter are especially interesting as the third block allows the formation of a broader variety of multicompartment microparticles (MMs), but their synthesis is often realized through sequential polymerization, which can be work intensive and challenging. Here, we demonstrate that blending linear ABC triblock terpolymers with homopolymers is a versatile and straightforward method to tune the microphase behavior in MMs. We systematically blend polystyrene-*block*-polybutadiene-*block*-poly(methyl methacrylate) (SBM or PS-*b*-PB-*b*-PM) with homopolymers of *h*PS, *h*PB, or *h*PM, to study the feasibility of this approach to replicate specific morphologies or access new ones. We utilize *Shirasu Porous Glass* (SPG) membrane emulsification and evaporation-induced confinement assembly (EICA) to produce narrowly size-dispersed MMs with defined inner structure. We analyze the MMs with dynamic light scattering (DLS), as well as transmission and scanning electron microscopy (TEM, SEM). We show that the resulting blend morphologies can be identical to those of the unblended SBM at same composition and that, depending on the location in the ternary microphase diagram, one SBM morphology can be converted into multiple different morphologies.

Keywords 3D confinement · ABC triblock terpolymers · Emulsification · Homopolymer blending · Microparticles · Morphology

Introduction

Block copolymers (BCPs) are a versatile class of soft matter, which consist of at least two covalently linked polymer blocks[1]. Due to the inherent incompatibility of the blocks that arises from differences in their chemical and physical properties, BCPs find widespread use in research and applications, including nanomedicine[2–6], catalysis[7, 8], compatibilization[9, 10], formation of mesoporous nanostructures[11–15] or energy storage[16, 17], to name a few examples. Irrespective of the intended use, control over the self-assembly or microphase behavior of BCPs is of vital importance for the quality and homogeneity of the final structure. While BCPs were primarily assembled in solution[18–23] or in bulk and at interfaces[24–32], their self-assembly in the confinement of emulsion droplets only recently gained traction[33–43]. There, the BCP is typically dissolved in an organic solvent and emulsified with an aqueous surfactant solution to create a (3D) spherical confinement for the BCP. During evaporation of the organic solvent, the droplet shrinks, which concentrates the BCP, and ultimately triggers the nucleation and growth of the BCP morphology. The resulting solid multicompartment microparticles (MMs) thereby develop characteristic shapes and internal morphologies dictated by the BCP composition. In addition, parameters such as

✉ André H. Gröschel
andre.groeschel@uni-bayreuth.de

1 Institute for Physical Chemistry and Center for Soft Nanoscience (SoN), University of Münster, Corrensstraße 28-30, 48149 Münster, Germany

2 Leibniz-Institut für Polymerforschung Dresden E.V, Hohe Straße 6, 01069 Dresden, Germany

3 Institut Für Theoretische Physik, Technische Universität Dresden, 01069 Dresden, Germany

4 Polymer Materials for Energy Storage (PES), Bavarian Centre for Battery Technology (BayBatt) and Bavarian Polymer Institute (BPI), University of Bayreuth, Universitätsstraße 30, 95448 Bayreuth, Germany

the rate of solvent evaporation[34, 44] and the affinity of the surfactant for certain blocks[36, 41, 45–49] can influence the orientation of the morphology and hence the shape of the MMs. This process allowed to produce *e.g.* hybrid particles[50], mesoporous structures[51–53], and photonic pigments[54–56].

While the morphological behavior of AB diblock copolymers in confinement is rather well understood, research on ABC triblock terpolymers is still comparably limited. The increased number of blocks and interaction parameters substantially increase the number of possible morphologies[1, 57]. The wealth of achievable morphologies can be mapped into ternary microphase diagrams, where subtle changes in block volume fraction can induce striking morphological transitions. Despite the appeal of largely increased morphological complexity, the introduction of a third block (and tuning its length) can be accompanied by time-consuming and complicated synthesis. Instead of synthesizing libraries of ABC triblock terpolymers, blending with homopolymers (*h*P) is an efficient and fast way to create large libraries of morphologies. If the *h*P has a comparatively low molecular weight, it swells the corresponding domain and increases its volume fraction (wet brush regime)[27, 58–61]. In contrast, blending with a *h*P of similar or higher molecular weight to the corresponding block prevents mixing and leads to phase separation of the *h*P instead (dry brush regime)[62–64]. The concept of blending was demonstrated for ABC triblock terpolymers in bulk as well as for AB diblock copolymers in confinement with the goal to obtain a certain structure or to study the microphase behavior[27, 60, 61, 63–65]. For blending of ABC triblock terpolymers in confinement, much less is known about targeting or altering specific morphologies.

In this work, we study the microphase behavior of polystyrene-*block*-polybutadiene-*block*-poly(methyl methacrylate) (SBM) in confinement for 6 block compositions, and systematically blend *h*PS, *h*PB, or *h*PM into the respective morphologies to study the effect of added volume on morphology. For emulsification, we use a Shirasu Porous Glass (SPG) membrane setup, leading to near-monodisperse MMs with controlled size. The overall shape and inner morphology of the MMs are analyzed by a combination of transmission and scanning electron microscopy (TEM, SEM). We show the possibility of replicating specific terpolymer morphologies, determine blending limits (*e.g.* excessive blending), and demonstrate the potential by transforming the morphology of one SBM into multiple other morphologies.

Materials and Methods

Materials. Analytical grade solvents and chemicals were used as received without further purification unless stated otherwise. Sodium dodecyl sulfate (SDS, > 99%), styrene, methyl methacrylate, 2-cyano-2-propyl dodecyl trithiocarbonate (CPDTC), 2,2'-azobis(2-methylpropionitrile) (azobisisobutyronitrile, AIBN) and polybutadiene homopolymer (*h*PB, $M_n = 2.0$ kg•mol^{-1}) were purchased from Sigma-Aldrich. The monomers were purified by running them over a silica column before use. OsO_4 was obtained from Science Services (OsO_4, 4 wt.% in H_2O) and ultrapure water from a Milli-Q® Integral Water Purification System. Regenerated cellulose tubes with a molecular weight cut-off of 12–14 kDa and an average flat width of 33 mm (Sigma Aldrich) were used for dialysis. The polystyrene-*block*-polybutadiene-*block*-poly(methyl methacrylate) triblock terpolymers (PS-*b*-PB-*b*-PM or SBM) were synthesized by sequential anionic polymerization as described previously[66].

Synthesis of PS and PM homopolymers. Both *h*P were synthesized with reversible addition-fragmentation chain transfer (RAFT) polymerization to control molecular weight, which was kept below the block lengths of the corresponding SBMs. For the synthesis of *h*PM, methyl methacrylate (6.2 mL, 58.4 mmol, 39 eq.) and CPDTC (505 mg, 1.5 mmol, 1 eq.) were dissolved in dioxane (30 mL) and a stock solution of AIBN in dioxane (1 g•L^{-1}) was prepared. Both solutions were bubbled with Argon for 20 min after which 24 µL of the AIBN solution (0.1 eq.) were added to the reaction vessel. The reaction mixture was stirred under Argon at 80 °C for 2 h before it was rapidly cooled with liquid nitrogen and exposed to air to stop the reaction. The polymer was precipitated in *n*-hexane. Residual solvent was removed under reduced pressure to obtain 1.8 g of *h*PM (2.7 kg•mol^{-1}, $Đ = 1.26$). For the synthesis of *h*PS, styrene (16.8 mL, 146.9 mmol, 92 eq.) and CPDTC (642 mg, 1.6 mmol, 1 eq.) were dissolved in anisole (10 mL) and a stock solution of AIBN in anisole (1 g•L^{-1}) was prepared. Both solutions were bubbled with Argon for 20 min after which 80 µL of the AIBN solution (0.3 eq.) were added to the reaction vessel. The reaction mixture was stirred under Argon at 80 °C for 2.75 h and then rapidly cooled with liquid nitrogen and exposed to ambient air to stop the reaction. The polymer was precipitated in *iso*-propanol. Residual solvent was removed under reduced pressure to obtain 4.8 g of *h*PS (3.0 kg•mol^{-1}, $Đ = 1.10$).

Fabrication of (blended) polymer particles with SPG-setup. The *h*P and SBM copolymers were separately dissolved in chloroform ($CHCl_3$) to prepare stock solutions ($c_{hP} = 20$ g•L^{-1} and $c_{SBM} = 10$ g•L^{-1}) that were mixed in varying ratios to achieve desired blend compositions. The specifics of SBM and SBM/*h*P are listed in Table 1 and a more detailed description on how these compositions were calculated can be found online in the Supplementary Information (SI). In a typical experiment, 1 mL of SBM or SBM/*h*P solution was emulsified in 20 mL of an aqueous SDS solution with a concentration of 5 g•L^{-1}. For that, the polymer solution was pushed through an SPG membrane with a pore diameter of 600 nm using pressurized Argon.

Table 1 SBM or SBM/hP used in this work

Polymer[a]	$Đ$[b]	Added vol% *h*P ($\approx\varphi_{hP}$)[c]	Final composition[d]	Morphology[e]	MM shape
$S_{32}B_{40}M_{28}{}^{125}$	1.05	-	$S_{32}B_{40}M_{28}{}^{125}$	*ll*	spherical
		+55% *h*PS ($\varphi_{PS}=0.18$)	$S_{50}B_{29}M_{21}$	*lpl*	spherical
$S_{50}B_{30}M_{20}{}^{159}$	1.09	-	$S_{50}B_{30}M_{20}{}^{159}$	*lpl*	spherical
$S_{59}B_{16}M_{25}{}^{119}$	1.11	-	$S_{59}B_{16}M_{25}{}^{119}$	*lr*	spherical
		+20% *h*PS ($\varphi_{PS}=0.11$)	$S_{70}B_{11}M_{19}$	c_oc	spherical
$S_{33}B_{23}M_{44}{}^{100}$	1.10	-	$S_{33}B_{23}M_{44}{}^{100}$	c_oc	spherical
		+20% *h*PS ($\varphi_{PS}=0.06$)	$S_{39}B_{21}M_{40}$	*lpl*	spherical
		+40% *h*PS ($\varphi_{PS}=0.13$)	$S_{46}B_{18}M_{36}$	*lr*	spherical
		+30% *h*PB ($\varphi_{PB}=0.06$)	$S_{30}B_{29}M_{41}$	c_oc/*ll*	prolate ellipsoid
		+55% *h*PB ($\varphi_{PB}=0.12$)	$S_{28}B_{35}M_{37}$	*ll*	prolate ellipsoid
		+15% *h*PM ($\varphi_{PM}=0.07$)	$S_{29}B_{20}M_{51}$	c_oc	spherical
		+25% *h*PM ($\varphi_{PM}=0.12$)	$S_{26}B_{18}M_{56}$	c_oc	spherical
$S_{41}B_{25}M_{34}{}^{143}$	1.09	-	$S_{41}B_{25}M_{34}{}^{143}$	*lpl*	prolate ellipsoid
		+50% *h*PS ($\varphi_{PS}=0.20$)	$S_{61}B_{16}M_{23}$	*lr*	prolate ellipsoid
$S_{74}B_{12}M_{14}{}^{89}$	1.06	-	$S_{74}B_{12}M_{14}{}^{89}$	c_oc	spherical
		+150% *h*PB ($\varphi_{PB}=0.17$)	$S_{60}B_{29}M_{11}$	c_oc/*hPB*	prolate-ellipsoid

[a] Subscripts are volume fractions of the blocks, φ_{ABC}, superscripts the M_n (kg•mol^{-1}) determined via SEC and ^{1}H-NMR. [b] Dispersity of SBM terpolymers obtained from SEC with PS standards in THF as eluent. [c] Added volume fraction φ_{hP}. [d] Final composition after blending φ_{ABC}. Subscripts denote the combined volume fraction of the block and *h*P; superscripts show the M_n of the original SBM. [e] Morphologies: *ll* = lamella-lamella, *lpl* = lamella-perforated lamella, *lr* = lamella-ring, c_oc = cylinder-on-cylinder

The emulsion was kept stirring at 250 rpm to yield droplets with a homogeneous size distribution. After stirring for five additional days, the organic solvent had evaporated, which resulted in the formation of solid MMs with inner structure. The MM suspension ($c=0.5$ g•L^{-1}) was dialyzed against ultrapure water to remove excess surfactant.

For SBM terpolymers, the volume fraction of the respective blocks is given in percent in the subscripts as φ_{ABC}, while the superscripts provide the number average molecular weight, M_n, in kg•mol^{-1}, determined by size exclusion chromatography (SEC). Blend compositions follow a similar definition, *i.e.*, subscripts refer to the final volume fraction φ_{ABC} in percent as a combination of the original φ_{ABC} plus added φ_{hP}. An overview of the SBMs and the SBM/*h*P used in this work is given in Table 1.

Transmission electron microscopy (TEM). To prepare TEM samples, MMs were first stained with Os by placing 1.2 mL of MM suspension in an open vial, which was then put in a chamber together with another open vial containing OsO_4 (4 wt.% in H_2O). The chamber was closed, and the liquids were kept under stirring for 3 h after which the chamber was opened. To remove excessive Os, the MMs were cleaned by centrifugation and redispersion in ultrapure water. A drop of the MM suspension ($c=0.5$ g•L^{-1}) was placed on a carbon-coated copper grid (400 mesh, Science Services) and excess liquid was blotted after 60 s using a filter paper. MMs were analyzed on a Talos L 120C (Thermo Fisher Scientific) with an acceleration voltage of 120 kV and an $LaBF_6$-filament. Images were taken with a Ceta-F camera and Velox Software (Version 3.8.80). The ImageJ open-source software package (Version 1.53 k) was used for processing the data[67]. Compartment sizes were measured and averaged over at least 50 different locations.

Scanning electron microscopy (SEM). A cryo-field emission SEM (Zeiss Cross Beam 340) equipped with an energy-selective detector for 16-bit image series acquisition with up to 40,000 × 50,000-pixel resolution and in lens chamber was used for SEM imaging. Samples for SEM measurements were prepared by putting one drop of an approximately 0.5 g·L^{-1} MM dispersion on a silicon wafer and dried for at least 4 h. The samples were then sputtered with 4 nm Au using a Quorum PP3010T-Cryo chamber with integrated Q150T-Es high-end sputter coater.

Size exclusion chromatography (SEC). Information about number-average molecular weight (M_n) and dispersity ($Đ=M_w/M_n$) were obtained by SEC. The polymer was dissolved in THF at a concentration of 1.5 g·L^{-1} and the solution was then filtered through a PTFE syringe filter (pore size of 0.2 µm) prior to being measured on a 1260 Infinity Instrument (PSS/Agilent, Mainz). The device was equipped with an isocratic pump, SDV PSS columns with porosities ranging from 10^2 – 10^6 Å, a differential refractometer, and a UV–Vis multiwavelength detector. For the synthesized *h*PS, PS standards were used for calibration (PSS/Agilent, Mainz) with molecular weights ranging from 1000 to 1 000 000 g·mol^{-1} and narrow size

distributions. For the synthesized *h*PM, PM standards were used in the same M_n-range.

Results and Discussion

Fabrication of MMs. All MMs (SBM or SBM/*h*P) were fabricated according to the following procedure. First, polymers were separately dissolved in chloroform ($CHCl_3$) at concentrations of $c_{SBM} = 10$ g•L^{-1} or $c_{hP} = 20$ g•L^{-1}. Depending on the desired blend composition, the SBM solution was mixed with a predetermined amount of *h*P solution. The mixture was then emulsified with an aqueous SDS solution ($c_{SDS} = 5$ g•L^{-1}) using the SPG membrane setup with a pore diameter of 600 nm. The organic solution was pushed through the membrane using pressurized Argon and the emulsion droplets were sheared off of the membrane by stirring. $CHCl_3$ evaporated over the course of several days under continuous stirring, which led to the formation of solid MMs. The blend compositions were chosen to move between areas of the ternary microphase diagram with known morphologies (unblended SBMs) to verify whether *h*P blending is able to replicate the morphology of one SBM by blending another. Of the investigated SBM terpolymers or SBM/*h*P blends, we were able to induce morphology transitions from lamella-lamella (*ll*) to lamella-perforated lamella (*lpl*), from *lpl* to lamella-ring (*lr*), from *lr* to cylinder-on-cylinder (c_oc), and from c_oc to *ll*, *lpl*, and *lr*. The morphologies will be discussed in more detail in the individual sections below. An overview of the SBM and SBM/*h*P morphologies in confinement can be found in Fig. 1.

Morphological transition through *h*PS blending. Here and in the following, we will move through the ternary microphase diagram shown in Fig. 1, starting in the cyan area (*ll*-morphology) and increase the *h*PS content towards the red area (c_oc-morphology), *i.e.*, we first transition from cyan to purple, then to dark blue and finally to red. We start by adding 55 vol% *h*PS relative to the PS block of $S_{32}B_{40}M_{28}$[125] equaling to an increase of $\varphi_{PS} = 0.18$ to reach a final composition of $S_{50}B_{29}M_{21}$ (Fig. 2a). According to DLS, all produced MMs show a monomodal and narrow size distribution of around $d_h \approx 600$ nm irrespective of blending (Figure S1). The addition of *h*PS (or any *h*P) does not negatively affect the stability of the emulsion droplets or disturb the microphase separation during MM solidification. The unblended $S_{32}B_{40}M_{28}$[125] originally formed spherical MMs with a concentric *ll*-morphology. The surface appears smooth (Fig. 2b) as PM forms the outermost shell, followed by a dark PB lamella (stained with OsO_4) and a thicker, gray PS lamella. This pattern (MBSSBM) alternates towards the center of the MM. This structure is expected as all blocks have similar volume fractions. After blending with *h*PS to $S_{50}B_{29}M_{21}$, we still find a concentric arrangement and a spherical MM (Fig. 2c), but the PB domain changed its appearance from a continuous lamella (dark line) to a discontinuous pattern (dark dotted line). The structural transition is induced as the

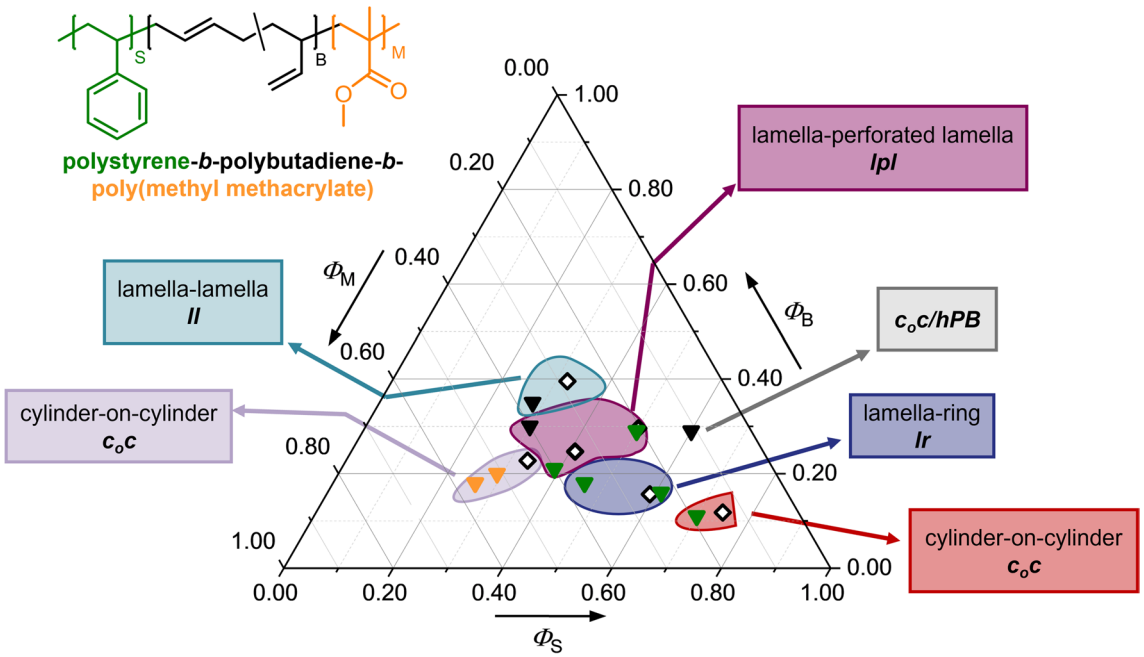

Fig. 1 Ternary microphase diagram of SBM and SBM/*h*P blends. The different morphologies are color coded. SBM morphologies are represented by empty diamonds, while SBM/*h*P blends are shown as filled triangles. The color of the triangle represents the homopolymer that was used for blending: green = *h*PS, black = *h*PB and orange = *h*PM

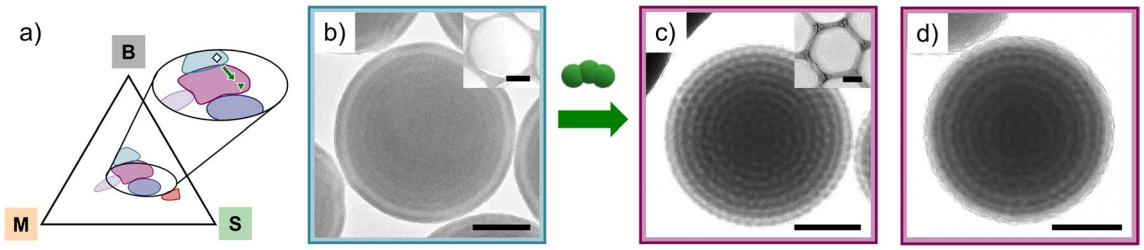

Fig. 2 Morphological transition of the *ll*-to *lpl*-morphology by blending of $S_{32}B_{40}M_{28}^{125}$ with 55 vol% *h*PS. a) Ternary microphase diagram with blending pathway indicated by the arrow. **b)** TEM image of $S_{32}B_{40}M_{28}^{125}$ MMs with *ll*-morphology (SEM in inset). **c)** TEM image of $S_{50}B_{29}M_{21}$ MMs with *lpl*-morphology after blending (SEM in inset). **d)** The *lpl*-morphology of $S_{50}B_{30}M_{20}^{159}$. PB was stained with OsO_4 and appears darkest. Scale bars are 200 nm

*h*PS accumulates in the PS domains, resulting in a distinct swelling of the PS lamellae, as evidenced by the increase of lamella width (w) from $w_{\text{lam, PS}} \approx 23$ nm to $w_{\text{lam, PS}} \approx 29$ nm. The incorporation of the *h*PS also leads to a relative decrease of φ_{PB} from 0.40 to 0.30, which lies below the *ll*-*lpl* transition value of around $\varphi_{\text{PB, } ll \leftrightarrow lpl} \approx 0.36$, so that PB forms a perforated lamella, yielding an *lpl*-morphology. [25, 60] Comparing this morphology with the unblended $S_{50}B_{30}M_{20}^{159}$ with similar volume fractions of the blocks, we also find the *lpl*-morphology (Fig. 2d)[60] with identical features as compared to the blended $S_{50}B_{29}M_{21}$. The main differences are the larger domain sizes that originate from the larger molecular weight of the unblended $S_{50}B_{30}M_{20}^{159}$. Blending thus allows to migrate between different areas of the ternary microphase diagram.

Blending does, however, has its limits as demonstrated by the addition of the relatively large 150 vol% *h*PB relative to the PB block of $S_{74}B_{12}M_{14}^{89}$, equaling to an increase of $\varphi_{\text{PB}} = 0.17$ to obtain $S_{60}B_{29}M_{11}$ (Figure S2a). There, we observed phase separation of the added *h*PB instead of blending. The morphology of $S_{74}B_{12}M_{14}^{89}$ can be ascribed to a cylinder-on-cylinder morphology within a PS matrix, as previously found for SBT triblock terpolymers with similar block volume fractions [43]. The blended $S_{60}B_{29}M_{11}$ retains the morphology, despite the increase of $\varphi_{\text{PB}} = 0.12$ to $\varphi_{\text{PB}} = 0.29$, mainly because the *h*PB accumulates at the tip of the MMs (Figure S2b). The *h*PB compartment can be clearly seen in TEM as dark collapsed areas, but also in the SEM as flattened or dimpled areas. This behavior was unexpected, as the $M \approx 2$ kg•mol^{-1} of the homopolymer is 5 times smaller than the $M_{\text{n, PB}} \approx 10$ kg•mol^{-1} of the PB block, and we therefor should be working in the wet brush regime [61, 68]. One explanation might be that the PB block has an overall small $\varphi_{\text{PB}} = 0.12$ and the microdomain may not be able to take up larger amounts of additional *h*PB before being saturated, *i.e.* the PB blocks are stretched to a critical threshold and unable to accommodate further *h*PB.

Knowing that larger volume fractions of *h*P will lead to phase separation, we continue our path in the ternary microphase diagram from the *lpl*-morphology (purple area) into the *lr*-morphology (dark blue area) by feeding PS into an unblended SBM (Fig. 3a). $S_{41}B_{25}M_{34}^{143}$ develops an *lpl*-morphology in elliptic MMs with axially stacked orientation (Fig. 3b). In the axially stacked case, PS/PM lamellae are clearly visible as linear stripes (discs), whereas the perforated lamellae of PB can be identified by a combination of dark dots and diagonal stripes. Compared to the spherical shape that we usually find for the MMs, the ellipsoidal

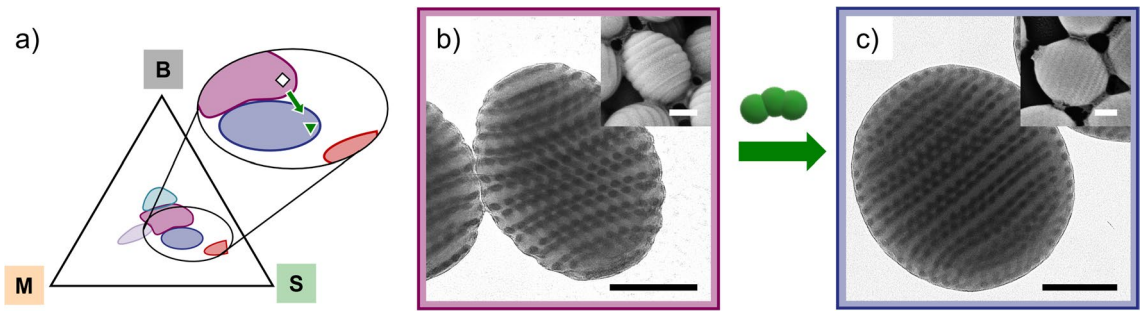

Fig. 3 Morphological transition of *lpl*- to *lr*-morphology by blending $S_{41}B_{25}M_{34}^{143}$ with 50 vol% *h*PS. a) Ternary microphase diagram with blending pathway indicated by the arrow. TEM and SEM (inset) images of **b)** unblended $S_{41}B_{25}M_{34}^{143}$ and **c)** $S_{61}B_{16}M_{23}$ blended with 50 vol% *h*PS. PB was stained with OsO_4 and appears darkest. Scale bars are 200 nm

shape and the axial stacking of the lamellae are likely caused by an interplay of two competing contributions. While the preferred interaction of the surfactant (here: SDS) with one of the blocks (here: the PM block) typically favors the spherical arrangement [36], a relatively high M_n (as in $S_{41}B_{25}M_{34}^{143}$) entropically impedes bending of the lamellae and therefor favors a flat, axially stacked arrangement. Blending $S_{41}B_{25}M_{34}^{143}$ with 50 vol% *h*PS relative to the PS block is equal to an increase in $\varphi_{PS} = 0.20$ to reach a final composition of $S_{61}B_{16}M_{23}$. This change in composition triggers a morphological transition of the PB microdomain into the *lr*-morphology. The thickness of the PS lamellae did not noticeably increase through blending (from 40 to 41 nm), but the lamella thickness is more homogeneous throughout the MM. The addition of low M_n *h*PS also appeared to cause a relaxation of the morphology, because the PS lamellae are more planar across the MM diameter instead of being bent, and the MM surface appears smoother than before in SEM and TEM.

As we continue to enrich the PS domain, we observed MM with a PS matrix, which requires the PB and PM microdomains to change their shape as well (Fig. 4). Addition of 20 vol% *h*PS relative to the PS block of $S_{59}B_{16}M_{25}^{119}$ is equal to an increase of $\varphi_{PS} = 0.11$ to obtain $S_{70}B_{11}M_{19}$. Since $S_{59}B_{16}M_{25}^{119}$ possess an *lr*-morphology (Fig. 4a), we expected the transition of at least two microdomains when φ_{PS} is increased [69]. Whereas the MMs still show a spherical structure with a smooth surface in SEM, TEM shows that PS now forms the matrix while PM changed into hexagonally packed cylinders (Fig. 4c). The PB domains maintain their cylindrical form and diameter, $d_{cyl,\ PB} \approx 15$ nm, resulting in an overall c_oc-morphology. The morphological change of PM is accompanied by an increase in the microdomain size from $d_{cyl\ PM} \approx 27$ nm in the blend compared to the thickness of the PM lamellae $w_{lam,\ PM} \approx 20$ nm before blending. Since the volume fraction φ_{PM} decreases during blending, an increase in PM domain size seems counterintuitive at first. However, the *total volume* of the PM block remains the same while the lamella microdomains separate into cylinders, which – at constant chain length – will result in a larger diameter.

Morphological transitions by blending *h*PS, *h*PB, or *h*PM. We next utilize $S_{33}B_{23}M_{44}^{100}$, whose composition resides within the c_oc-morphology with PB cylinders on PS cylinders embedded in a PM matrix (Fig. 5a, b), but is likewise located near the *lpl* region (blue region in Fig. 5a) and the *ll* region (purple region in Fig. 5a). Thus, multiple transitions could be expected after blending. First, we blended $S_{33}B_{23}M_{44}^{100}$ with *h*PS to obtain $S_{39}B_{21}M_{40}$ (20 vol%; $\varphi_{PS} = 0.06$) and $S_{46}B_{18}M_{36}$ (40 vol%; $\varphi_{PS} = 0.13$). The morphology of $S_{39}B_{21}M_{40}$ already shows signs of change towards an *lpl*-morphology but is still in a transition state so that the MM appears disordered (Figure S3)[70]. While merging of PS cylinders into lamellae takes place to some extent, the added *h*PS is not sufficient to induce a full transition. Blending a larger amount of *h*PS to reach $S_{46}B_{18}M_{36}$ fully realized the transition and continuous PS lamellae are observed (Fig. 5c). During merging of cylinders, the PS domain decreases in thickness from cylinders with a diameter of $d_{cyl,\ PS} \approx 40$ nm to lamellae with a width of $w_{lam,\ PS} \approx 25$ nm. At the same time, the PM matrix adopts a lamella morphology as well, and PB now forms rings instead of straight cylinders due to the concentric PS/PM lamellae.

Next, we blended $S_{33}B_{23}M_{44}^{100}$ with *h*PM to obtain $S_{29}B_{20}M_{51}$ (15 vol%; $\varphi_{PM} = 0.07$; Fig. 5d) and $S_{26}B_{18}M_{56}$ (25 vol%; $\varphi_{PM} = 0.12$; Figure S3d). Both blends led to a c_oc morphology, but now the packing of PS domains is clearly hexagonal instead of tetragonal. The PB cylinders are at the interface between the PS cylinders and the PM matrix. Even though we did not observe a change in the microdomains, the results demonstrate that blending also allows to induce rather subtle changes in morphologies, making it a powerful tool for finetuning. Finally, we blended $S_{33}B_{23}M_{44}^{100}$ with *h*PB to $S_{30}B_{29}M_{40}$ (30 vol%;$\varphi_{PB} = 0.06$; Figure S3e) and $S_{28}B_{35}M_{37}$ (55 vol%; $\varphi_{PB} = 0.12$; Fig. 5e). In these blended compositions, all blocks have about equal volume fractions for which

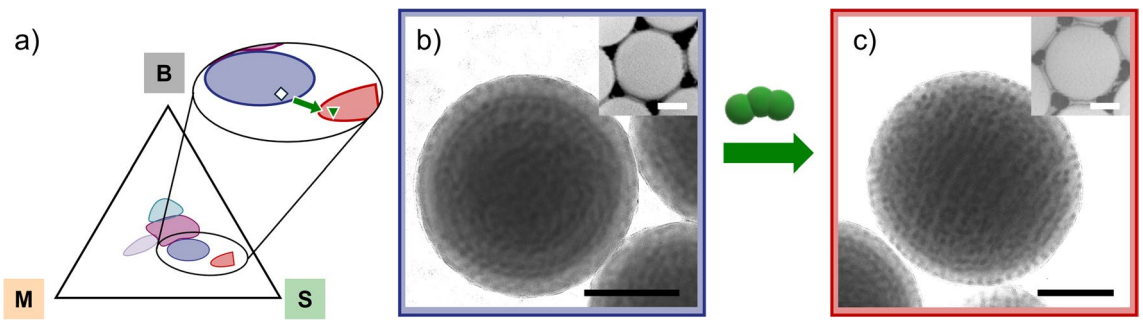

Fig. 4 Blending of $S_{59}B_{16}M_{25}^{119}$ with 20 vol% *h*PS. a) Ternary microphase diagram with blending pathway indicated by the arrow. **b)** TEM and SEM (inset) images of unblended $S_{59}B_{16}M_{25}^{119}$ and **c)** of $S_{70}B_{11}M_{19}$ blended with 20 vol% *h*PS. PB was stained with OsO_4 and appears darkest. Scale bars are 200 nm

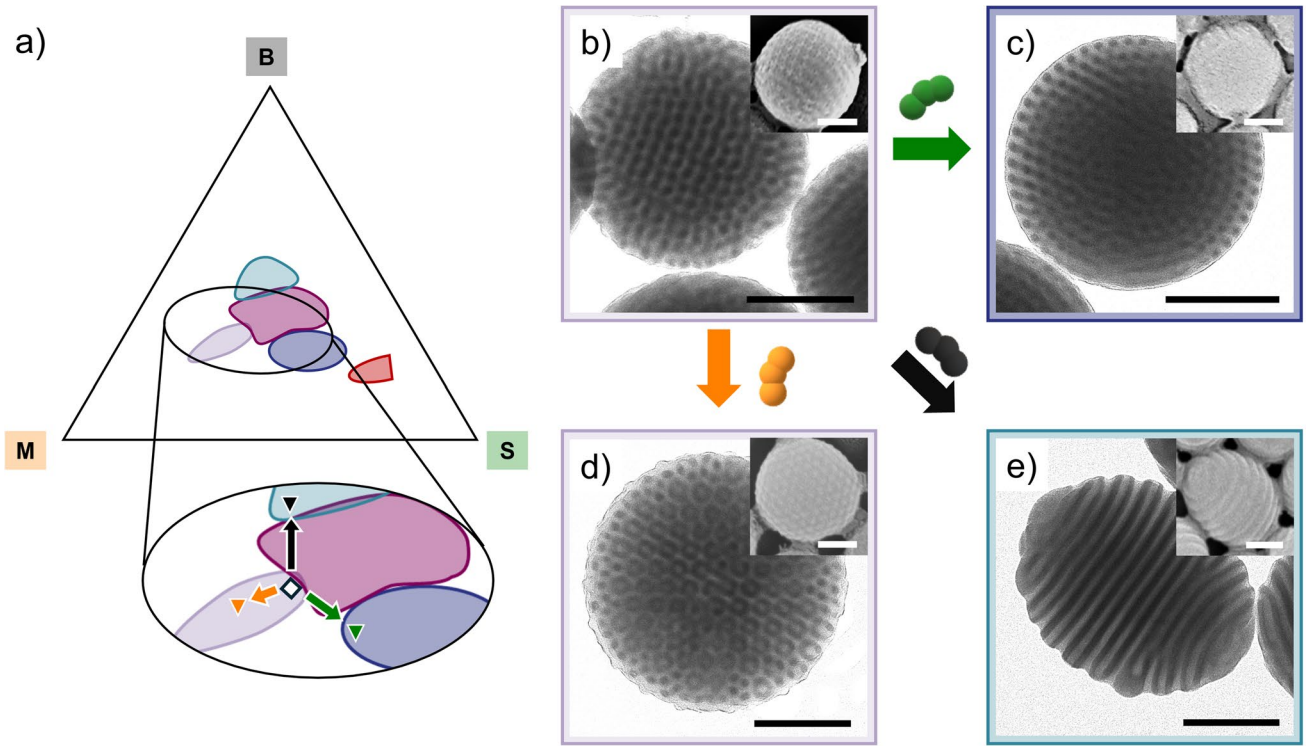

Fig. 5 Structural transitions of blended $S_{33}B_{23}M_{44}^{100}$. a) Ternary microphase diagram with blending pathway indicated in the closeup. TEM and SEM (inset) images of **b)** unblended $S_{33}B_{23}M_{44}^{100}$, **c)** *h*PS blended $S_{46}B_{18}M_{36}$, **d)** *h*PM blended $S_{29}B_{20}M_{51}$, and **e)** *h*PB blended $S_{28}B_{35}M_{37}$. PB was stained with OsO_4 and appears darkest. Scale bars are 200 nm

a transition to the *ll*-morphology is expected. For $S_{30}B_{29}M_{40}$ (Figure S3e), we already partially see this trend, *i.e.*, PS and PM clearly transition to lamellae, while PB mostly forms perforated lamellae, leading to the *lpl*-morphology. Again, the addition of more *h*PB led to continuous PB lamellae and a homogeneous axially stacked *ll*-morphology (Fig. 5e). Merging of PB cylinders towards lamellae is accompanied by merging of PS cylinders into lamellae with a thickness of $w_{PS} \approx 18$ nm. Since no PS was added to the system, the decrease in PS domain size is more pronounced than discussed above ($S_{46}B_{18}M_{36}^{100}$, Fig. 5c). In comparison, the decrease of the PB domain size is rather small, *i.e.*, the width of the lamellae, $w_{PB} \approx 17$ nm, is only about 2 nm smaller than the diameter of the PB cylinders found for $S_{33}B_{23}M_{44}^{100}$.

Conclusions

In conclusion, we showed that blending linear SBM triblock terpolymers with homopolymers is an effective strategy for tuning the inner structure of terpolymer-based multicompartment microparticles. We induced and analyzed one-, two- or three-compartment-transitions in the particle morphologies and demonstrated the versatility and potential of this approach. In parallel, we investigated possible issues and limitations related to over-blending of the homopolymer, such as phase separation of the added homopolymers. Our results demonstrate that this blending approach successfully replicates the morphologies of pure SBM terpolymers, thereby avoiding the time- and cost-intensive synthesis of different terpolymer compositions. Looking ahead, we aim to further leverage the acquired knowledge and potential for the structural analysis of triblock terpolymer based microparticles and the establishment of a ternary microphase diagram as a comprehensive guideline for targeting specific morphologies. Future research will also investigate the simultaneous blending with two homopolymers to expand the scope of this approach.

Supplementary Information The online version contains supplementary material available at https://doi.org/10.1007/s00396-024-05320-4.

Acknowledgements For SEM imaging the authors made use of Münster Nanofabrication Facility (MNF). Y. Post is acknowledged for DLS measurements. Part of this work was performed at the SoN – cryo-EM platform supported by the German Research Foundation (DFG), INST 211/1048-1 FUGG and the University of Muenster. This work was supported by the DFG through projects 445740352 and 470113688.

Author Contributions Data was acquired and visualized by MT. AHG and AN conceived the project, acquired funding, and supervised the project. The manuscript was written through contributions of all authors. All authors have given approval to the final version of the manuscript.

Funding Open Access funding enabled and organized by Projekt DEAL. This work was supported by the German Research Foundation (projects 445740352 and 470113688).

Data Availability No datasets were generated or analysed during the current study.

Declarations

Ethical Approval Not applicable.

Conflict of Interest The authors declare no conflict of interest.

References

1. Bates FS, Fredrickson GH (1999) Block copolymers-designer soft materials. Phys Today 52:32–38. https://doi.org/10.1063/1.882522
2. Moulahoum H, Ghorbanizamani F, Zihnioglu F, Timur S (2021) Surface Biomodification of Liposomes and Polymersomes for Efficient Targeted Drug Delivery. Bioconjug Chem 32:1491–1502. https://doi.org/10.1021/acs.bioconjchem.1c00285
3. Sinsinbar G, Kaur Bindra A, Liu S, Wan Chia T, Chia YoongEng E, Yue Loo S et al (2024) Amphiphilic Block Copolymer Nanostructures as a Tunable Delivery Platform: Perspective and Framework for the Future Drug Product Development. Biomacromolecules 25:541–63. https://doi.org/10.1021/acs.biomac.3c00858
4. Cabral H, Miyata K, Osada K, Kataoka K (2018) Block Copolymer Micelles in Nanomedicine Applications. Chem Rev 118:6844–6892. https://doi.org/10.1021/acs.chemrev.8b00199
5. Synatschke CV, Nomoto T, Cabral H, Förtsch M, Toh K, Matsumoto Y et al (2014) Multicompartment Micelles with Adjustable Poly(ethylene glycol) Shell for Efficient in Vivo Photodynamic Therapy. ACS Nano 8:1161–1172. https://doi.org/10.1021/nn4028294
6. Pagels RF, Prud'homme RK (2015) Polymeric nanoparticles and microparticles for the delivery of peptides, biologics, and soluble therapeutics. J Control Release 219:519–35. https://doi.org/10.1016/j.jconrel.2015.09.001
7. Ahmed E, Cho J, Friedmann L, Soon Jang S, Weck M (2022) Catalytically Active Multicompartment Micelles. JACS Au 2:2316–2326. https://doi.org/10.1021/jacsau.2c00367
8. Nghiem TL, Coban D, Tjaberings S, Gröschel AH (2020) Recent advances in the synthesis and application of polymer compartments for catalysis. Polymers (Basel) 12(10):2190. https://doi.org/10.3390/POLYM12102190
9. Zhou T, Ning X, Wu Z, Lan X, Xu C (2024) Understanding the Interfacial and Self-Assembly Behavior of Multiblock Copolymers for Developing Compatibilizers toward Mechanical Recycling of Polymer Blends. Ind Eng Chem Res 63:6766–6773. https://doi.org/10.1021/acs.iecr.3c03944
10. Self JL, Zervoudakis AJ, Peng X, Lenart WR, Macosko CW, Ellison CJ (2022) Linear, Graft, and Beyond: Multiblock Copolymers as Next-Generation Compatibilizers. JACS Au 2:310–321. https://doi.org/10.1021/jacsau.1c00500
11 Grandes Reyes CF, Ha S, Kim KT (2023) Synthesis and applications of polymer cubosomes and hexosomes. J Polym Sci 61:1196–213. https://doi.org/10.1002/pol.20230053
12. Gröschel AH, Walther A (2017) Block Copolymer Micelles with Inverted Morphologies. Angew Chem Int Ed 56:10992–4. https://doi.org/10.1002/anie.201703765
13. Gemmer L, Niebuur BJ, Dietz C, Rauber D, Plank M, Frieß FV et al (2023) Polyacrylonitrile-containing amphiphilic block copolymers: self-assembly and porous membrane formation. Polym Chem 14:4825–4837. https://doi.org/10.1039/d3py00836c
14. Radjabian M, Abetz V (2020) Advanced porous polymer membranes from self-assembling block copolymers. Prog Polym Sci 102:101219. https://doi.org/10.1016/J.PROGPOLYMSCI.2020.101219
15. Wang H, Shao Y, Mei S, Lu Y, Zhang M, Sun JK et al (2020) Polymer-Derived Heteroatom-Doped Porous Carbon Materials. Chem Rev 120:9363–9419. https://doi.org/10.1021/acs.chemrev.0c00080
16. Li W, Liu J, Zhao D (2016) Mesoporous materials for energy conversion and storage devices. Nat Rev Mater 1:16023. https://doi.org/10.1038/natrevmats.2016.23
17. Li C, Li Q, Kaneti YV, Hou D, Yamauchi Y, Mai Y (2020) Self-assembly of block copolymers towards mesoporous materials for energy storage and conversion systems. Chem Soc Rev 49:4681–4736. https://doi.org/10.1039/D0CS00021C
18. Mai Y, Eisenberg A (2012) Self-assembly of block copolymers. Chem Soc Rev 41:5969–5985. https://doi.org/10.1039/c2cs35115c
19. Löbling TI, Borisov O, Haataja JS, Ikkala O, Gröschel AH, Müller AHE (2016) Rational design of ABC triblock terpolymer solution nanostructures with controlled patch morphology. Nat Commun 7(1):12097. https://doi.org/10.1038/ncomms12097
20. Gröschel AH, Walther A, Löbling TI, Schacher FH, Schmalz H, Müller AHE (2013) Guided hierarchical co-assembly of soft patchy nanoparticles. Nature. 503:247–51. https://doi.org/10.1038/nature12610
21. Hua Z, Jones JR, Thomas M, Arno MC, Souslov A, Wilks TR et al (2019) Anisotropic polymer nanoparticles with controlled dimensions from the morphological transformation of isotropic seeds. Nat Commun 10(1):5406. https://doi.org/10.1038/s41467-019-13263-6
22. Johnson BK, Prud'homme RK (2003) Mechanism for rapid self-assembly of block copolymer nanoparticles. Phys Rev Lett 91(11):118302. https://doi.org/10.1103/PhysRevLett.91.118302
23. Rodríguez-Hernández J, Chécot F, Gnanou Y, Lecommandoux S (2005) Toward 'smart' nano-objects by self-assembly of block copolymers in solution. Prog Polym Sci 30:691–724. https://doi.org/10.1016/J.PROGPOLYMSCI.2005.04.002
24. Brinkmann S, Stadler R, L. (1998) Thomas E. New Structural Motif in Hexagonally Ordered Cylindrical Ternary (ABC) Block Copolymer Microdomains. Macromolecules 31:6566–72. https://doi.org/10.1021/ma980103q
25. Krappe U, Stadler R, Voigt-Martin I (1995) Chiral Assembly in Amorphous ABC Triblock Copolymers. Formation of a Helical Morphology in Polystyrene-block-polybutadiene-block-poly(methyl methacrylate) Block Copolymers. Macromolecules 28:4558–61. https://doi.org/10.1021/ma00117a027
26. Stadler R, Auschra C, Beckmann J, Krappe U, Voigt-Martin I, Leibler L (1995) Morphology and Thermodynamics of Symmetric

Poly(A-block-B-block-C) Triblock Copolymers. Macromolecules 28:3080–97. https://doi.org/10.1021/ma00113a010
27. Steinhaus A, Srivastva D, Nikoubashman A, Gröschel AH (2019) Janus Nanostructures from ABC/B Triblock Terpolymer Blends. Polymers 11:1107. https://doi.org/10.3390/POLYM11071107
28. Breiner U, Krappe U, Jakob T, Abetz V, Stadler R (1998) Spheres on spheres-a novel spherical multiphase morphology in polystyrene-block-polybutadiene-block-poly(methyl methacrylate) triblock copolymers. Polym Bull 40:219–26. https://doi.org/10.1007/s002890050245
29. Breiner U, Krappe U, Abetz V, Stadler R (1997) Cylindrical morphologies in asymmetric ABC triblock copolymers. Macromol Chem Phys 198:1051–1083. https://doi.org/10.1002/macp.1997.021980411
30. Auschra C, Stadler R (1993) New ordered morphologies in ABC triblock copolymers. Macromolecules 26:2171–2174. https://doi.org/10.1021/ma00061a005
31. Gon Son J, Gwyther J, Chang J-B, K. Berggren K, Manners I, A. Ross C. 2011 Highly Ordered Square Arrays from a Templated ABC Triblock Terpolymer. Nano Lett. 11:2849–55. https://doi.org/10.1021/nl201262f
32. Löbling TI, Hiekkataipale P, Hanisch A, Bennet F, Schmalz H, Ikkala O et al (2015) Bulk morphologies of polystyrene-block-polybutadiene-block-poly(tert-butyl methacrylate) triblock terpolymers. Polymer (Guildf) 72:479–489. https://doi.org/10.1016/j.polymer.2015.02.025
33. Tan Z, Kim EJ, Li S, Hur SM, Shin JJ, Kim BJ (2024) Shape-Controlled Anisotropic Block Copolymer Particles via Interfacial Engineering of Multiple-Phase Emulsions. Macromolecules. https://doi.org/10.1021/acs.macromol.4c00668
34. Shin JM, Kim Y, Yun H, Yi G-R, Kim BJ (2017) Morphological Evolution of Block Copolymer Particles: Effect of Solvent Evaporation Rate on Particle Shape and Morphology. ACS Nano 11:38. https://doi.org/10.1021/acsnano.6b08342
35. Lee J, Ku KH, Kim M, Shin JM, Han J, Park CH et al (2017) Stimuli-Responsive, Shape-Transforming Nanostructured Particles. Adv Mater 29:1700608. https://doi.org/10.1002/adma.201700608
36. Trömer M, Zirdehi EM, Nikoubashman A, Gröschel AH (2023) Effect of Surfactant Selectivity on Shape and Inner Morphology of Triblock Terpolymer Microparticles. Macromol Rapid Commun. https://doi.org/10.1002/marc.202300123
37. Zhang M, Hou Z, Wang H, Zhang L, Xu J, Zhu J (2021) Shaping Block Copolymer Microparticles by pH-Responsive Core-Cross-Linked Polymeric Nanoparticles. Langmuir 37:454–460. https://doi.org/10.1021/acs.langmuir.0c03099
38. Xu J, Wang K, Li J, Zhou H, Xie X, Zhu J (2015) ABC Triblock Copolymer Particles with Tunable Shape and Internal Structure through 3D Confined Assembly. Macromolecules 48:2628–2636. https://doi.org/10.1021/acs.macromol.5b00335
39. Jang SG, Audus DJ, Klinger D, Krogstad DV, Kim BJ, Cameron A et al (2013) Striped, ellipsoidal particles by controlled assembly of diblock copolymers. J Am Chem Soc 135:6649–6657. https://doi.org/10.1021/ja4019447
40. Navarro L, Thünemann AF, Yokosawa T, Spiecker E, Klinger D. Regioselective Seeded Polymerization in Block Copolymer Nanoparticles: Post-Assembly Control of Colloidal Features. 2022 Angewandte Chemie - International Edition 61. https://doi.org/10.1002/ANIE.202208084
41. Klinger D, Wang CX, Connal LA, Audus DJ, Jang SG, Kraemer S et al (2014) A Facile Synthesis of Dynamic, Shape-Changing Polymer Particles. Angew Chem Int Ed 53:7018–7022. https://doi.org/10.1002/anie.201400183
42. Qiang X, Chakroun R, Janoszka N, Gröschel AH (2019) Self-Assembly of Multiblock Copolymers. Isr J Chem 59:945–958. https://doi.org/10.1002/ijch.201900044
43. Qiang X, Franzka S, Dai X, H. Gröschel A. 2020 Multicompartment Microparticles of SBT Triblock Terpolymers through 3D Confinement Assembly. Macromolecules. 53:4224–33. https://doi.org/10.1021/acs.macromol.0c00806
44. Shin JM, Kim MP, Yang H, Hee KuK, Gyu Jang S, Ho Youm K et al (2015) Monodipserse Nanostructured Spheres of Block Copolymers and Nanoparticles via Cross-Flow Membrane Emulsification. Chem Mater 27:6314–6321. https://doi.org/10.1021/acs.chemmater.5b02020
45. Huang C, Zhang X, Lyu X (2024) Encounter between Gyroid and Lamellae in Janus Colloidal Particles Self-Assembled by a Rod-Coil Block Copolymer. Macromol Rapid Commun. https://doi.org/10.1002/marc.202300696
46. Navarro L, Thünemann AF, Klinger D (2022) Solvent Annealing of Striped Ellipsoidal Block Copolymer Particles: Reversible Control over Lamellae Asymmetry, Aspect Ratio, and Particle Surface. ACS Macro Lett 11:329–335. https://doi.org/10.1021/acsmacrolett.1c00665
47. Yang S, Cao Y, Wang S, Li Y, Shi J (2022) Understanding on the Surfactants Engineered Morphology Evolution of Block Copolymer Particles and Their Precise Mesoporous Silica Replicas. Chem Res Chin Univ 38:99–106. https://doi.org/10.1007/s40242-021-1403-0
48. Kim J, Lee YJ, Ku KH, Kim BJ (2022) Effect of Molecular Structure of Photoswitchable Surfactant on Light-Responsive Shape Transition of Block Copolymer Particles. Macromolecules 55:8355–8364. https://doi.org/10.1021/acs.macromol.2c01465
49. Lee J, Ku KH, Kim J, Lee YJ, Jang SG, Kim BJ (2019) Light-Responsive, Shape-Switchable Block Copolymer Particles. J Am Chem Soc 141:15348–15355. https://doi.org/10.1021/jacs.9b07755
50. Kim MP, Yi GR (2015) Nanostructured colloidal particles by confined self-assembly of block copolymers in evaporative droplets. Front Mater 2:1. https://doi.org/10.3389/fmats.2015.00045
51. Janoszka N, Azhdari S, Hils C, Coban D, Schmalz H, Gröschel AH (2021) Morphology and Degradation of Multicompartment Microparticles Based on Semi-Crystalline Polystyrene-block-Polybutadiene-block-Poly(L-lactide) Triblock Terpolymers. Polymers (Basel) 13:4358. https://doi.org/10.3390/polym13244358
52. Jun Lee Y, Kim H-E, Oh H, Yun H, Lee J, Shin S et al (2022) Lens-Shaped Carbon Particles with Perpendicularly-Oriented Channels for High-Performance Proton Exchange Membrane Fuel Cells. ACS Nano 16:2988–2996. https://doi.org/10.1021/acsnano.1c10280
53. Li H, Mao X, Wang H, Geng Z, Xiong B, Zhang L et al (2020) Kinetically Dependent Self-Assembly of Chiral Block Copolymers under 3D Confinement. Macromolecules 53:4214–4223. https://doi.org/10.1021/acs.macromol.0c00406
54 He Q, Ku KH, Vijayamohanan H, Kim BJ, Swager TM (2020) Switchable Full-Color Reflective Photonic Ellipsoidal Particles. J Am Chem Soc 142:10424–30. https://doi.org/10.1021/jacs.0c02398
55. Yang Y, Kim H, Xu J, Hwang MS, Tian D, Wang K et al (2018) Responsive Block Copolymer Photonic Microspheres. Adv Mater 30(21):1707344. https://doi.org/10.1002/adma.201707344
56 Wang Z, Chan CLC, Zhao TH, Parker RM, Vignolini S (2021) Recent Advances in Block Copolymer Self-Assembly for the Fabrication of Photonic Films and Pigments. Adv Opt Mater 9(21):2100519. https://doi.org/10.1002/adom.202100519
57. Bates FS, Hillmyer MA, Lodge TP, Bates CM, Delaney KT, Fredrickson GH (2012) Multiblock Polymers: Panacea or Pandora's

Box? Science 336(6080):434-440. https://doi.org/10.1126/science.1215368
58. Koizumi S, Hasegawa H, Hashimoto T (1994) Ordered Structures of Block Copolymer/Homopolymer Mixtures. 5 Interplay of Macro-and Microphase Transitions. Macromolecules 27:6532–40. https://doi.org/10.1021/MA00100A044
59. Hashimoto T, Tanaka H, Hasegawa H (1990) Ordered Structure in Mixtures of a Block Copolymer and Homopolymers. 2. Effects of Molecular Weights of Homopolymers. Macromolecules 23:4378–86. https://doi.org/10.1021/MA00222A009
60. Steinhaus A, Srivastva D, Qiang X, Franzka S, Nikoubashman A, Gröschel AH (2021) Controlling Janus Nanodisc Topology through ABC Triblock Terpolymer/Homopolymer Blending in 3D Confinement. Macromolecules 54:1224–1233. https://doi.org/10.1021/acs.macromol.0c02769
61. Xu J, Yang Y, Wang K, Li J, Zhou H, Xie X et al (2015) Additives Induced Structural Transformation of ABC Triblock Copolymer Particles. Langmuir 31:10975–10982. https://doi.org/10.1021/acs.langmuir.5b02843
62. Hashimoto T, Koizumi S, Hasegewa H (1995) Interfaces in block copolymer/homopolymer mixtures forming dry brushes. Physica B Condens Matter 213–214:676–681. https://doi.org/10.1016/0921-4526(95)00247-7
63. Azhdari S, Post Y, Trömer M, Coban D, Quintieri G, Gröschel AH (2023) Janus nanoplates, -bowls, and -cups: controlling size and curvature via terpolymer/homopolymer blending in 3D confinement. Nanoscale. https://doi.org/10.1039/d3nr02902f
64. Qiang X, Steinhaus A, Chen C, Chakroun R, Gröschel AH (2019) Template-Free Synthesis and Selective Filling of Janus Nanocups. Angew Chem Int Ed 58:7122–7126. https://doi.org/10.1002/anie.201814014
65. Higuchi T, Sugimori H, Jiang X, Hong S, Matsunaga K, Kaneko T et al (2013) Morphological control of helical structures of an ABC-type triblock terpolymer by distribution control of a blending homopolymer in a block copolymer microdomain. Macromolecules 46:6991–6997. https://doi.org/10.1021/MA401193U
66. Auschra C, Stadler R (1993) Synthesis of block copolymers with poly(methyl methacrylate): P(B-b-MMA), P(EB-b-MMA), P(S-b-B-b-MMA) and P(S-b-EB-b-MMA). Polym Bull 30:257–264. https://doi.org/10.1007/BF00343058
67. Schindelin J, Arganda-Carreras I, Frise E, Kaynig V, Longair M, Pietzsch T et al (2012) Fiji: an open-source platform for biological-image analysis. Nat Methods 9:676–682. https://doi.org/10.1038/nmeth.2019
68. Yabu H, Sato S, Higuchi T, Jinnai H, Shimomura M (2012) Creating suprapolymer assemblies: Nanowires, nanorings, and nanospheres prepared from symmetric block-copolymers confined in spherical particles. J Mater Chem 22:7672–7675. https://doi.org/10.1039/c2jm30236e
69. Steinhaus A, Chakroun R, Müllner M, Nghiem TL, Hildebrandt M, Gröschel AH (2019) Confinement Assembly of ABC Triblock Terpolymers for the High-Yield Synthesis of Janus Nanorings. ACS Nano 13:6269–6278. https://doi.org/10.1021/ACSNANO.8B09546
70. Sakurai S, Momii T, Taie K, Shibayama M, Nomura S, Takeji Hashimoto J (1993) Morphology Transition from Cylindrical to Lamellar Microdomains of Block Copolymers. Macromolecules. 26:485–91. https://doi.org/10.1021/ma00055a013